NASA/CR—2013-218090

# Jet Surface Interaction—Scrubbing Noise

*Abbas Khavaran*
*Vantage Partners, LLC, Cleveland, Ohio*

September 2013

# NASA STI Program . . . in Profile

Since its founding, NASA has been dedicated to the advancement of aeronautics and space science. The NASA Scientific and Technical Information (STI) program plays a key part in helping NASA maintain this important role.

The NASA STI Program operates under the auspices of the Agency Chief Information Officer. It collects, organizes, provides for archiving, and disseminates NASA's STI. The NASA STI program provides access to the NASA Aeronautics and Space Database and its public interface, the NASA Technical Reports Server, thus providing one of the largest collections of aeronautical and space science STI in the world. Results are published in both non-NASA channels and by NASA in the NASA STI Report Series, which includes the following report types:

- TECHNICAL PUBLICATION. Reports of completed research or a major significant phase of research that present the results of NASA programs and include extensive data or theoretical analysis. Includes compilations of significant scientific and technical data and information deemed to be of continuing reference value. NASA counterpart of peer-reviewed formal professional papers but has less stringent limitations on manuscript length and extent of graphic presentations.

- TECHNICAL MEMORANDUM. Scientific and technical findings that are preliminary or of specialized interest, e.g., quick release reports, working papers, and bibliographies that contain minimal annotation. Does not contain extensive analysis.

- CONTRACTOR REPORT. Scientific and technical findings by NASA-sponsored contractors and grantees.

- CONFERENCE PUBLICATION. Collected papers from scientific and technical conferences, symposia, seminars, or other meetings sponsored or cosponsored by NASA.

- SPECIAL PUBLICATION. Scientific, technical, or historical information from NASA programs, projects, and missions, often concerned with subjects having substantial public interest.

- TECHNICAL TRANSLATION. English-language translations of foreign scientific and technical material pertinent to NASA's mission.

Specialized services also include creating custom thesauri, building customized databases, organizing and publishing research results.

For more information about the NASA STI program, see the following:

- Access the NASA STI program home page at *http://www.sti.nasa.gov*

- E-mail your question to *help@sti.nasa.gov*

- Fax your question to the NASA STI Information Desk at 443–757–5803

- Phone the NASA STI Information Desk at 443–757–5802

- Write to:
  STI Information Desk
  NASA Center for AeroSpace Information
  7115 Standard Drive
  Hanover, MD 21076–1320

NASA/CR—2013-218090

# Jet Surface Interaction—Scrubbing Noise

*Abbas Khavaran*
*Vantage Partners, LLC, Cleveland, Ohio*

Prepared under Contract NNC12BA01B

National Aeronautics and
Space Administration

Glenn Research Center
Cleveland, Ohio 44135

September 2013

## Acknowledgments

This work was sponsored by the NASA Fundamental Aeronautics Program. The author is grateful to the Acoustics Branch at NASA Glenn Research Center for supporting this research effort, and to Dr. Stewart Leib for his very insightful comments and suggestions.

This report is a formal draft or working paper, intended to solicit comments and ideas from a technical peer group.

This report contains preliminary findings, subject to revision as analysis proceeds.

This work was sponsored by the Fundamental Aeronautics Program at the NASA Glenn Research Center.

*Level of Review*: This material has been technically reviewed by NASA technical management OR expert reviewer(s).

Available from

NASA Center for Aerospace Information
7115 Standard Drive
Hanover, MD 21076–1320

National Technical Information Service
5301 Shawnee Road
Alexandria, VA 22312

Available electronically at http://www.sti.nasa.gov

# Jet Surface Interaction—Scrubbing Noise

Abbas Khavaran
Vantage Partners, LLC
Cleveland, Ohio 44135

**Abstract**

Generation of sound due to scrubbing of a jet flow past a nearby solid surface is investigated within the framework of the generalized acoustic analogy theory. The analysis applies to the boundary layer noise generated at and near a wall, and excludes the scattered noise component that is produced at the leading or the trailing edge. While compressibility effects are relatively unimportant at very low Mach numbers, frictional heat generation and thermal gradient normal to the surface could play important roles in generation and propagation of sound in high speed jets of practical interest. A general expression is given for the spectral density of the far-field sound as governed by the variable density Pridmore-Brown equation. The propagation Green's function should be solved numerically starting with the boundary conditions on the surface and subject to specified mean velocity and temperature profiles between the surface and the observer. The equivalent sources of aerodynamic sound are associated with non-linear momentum flux and enthalpy flux terms that appear in the linearized Navier-Stokes equations. These multi-pole sources should be modeled and evaluated with input from a Reynolds-Averaged Navier-Stokes (RANS) solver with an appropriate turbulence model.

## 1.0 Introduction

The Fundamental Aeronautics program at NASA faces new technological challenges in order to meet recent air transportation rules that include reduced noise, emission, and fuel consumption. The U.S. commercial aviation is projected to increase by 70% in the period 2010 – 2030, resulting in more exposure to air traffic noise in the communities surrounding airports. Recent noise metrics require a cumulative (cutback, sideline, and approach) noise reduction in the subsonic transport of 32dB by 2015 and 52dB by 2025 (referenced to 737-800 aircraft with CFM56-7B engines). In 2008, NASA instigated a call for conceptual design of future commercial transport in order to meet specific goals related to noise, air pollution, and fuel consumption. Early studies indicated that both propulsion system and engine placement have to be modified in order to achieve these new objectives. In particular, placement of the aircraft engine for the purpose of reduced community noise poses new challenges in structural design, material selection as well as computations. Configurations such as over the wing engine mount (Fig. 1), distributed propulsion, Hybrid Wing Body (HWB) concept, and/or high aspect-ratio rectangular exhaust geometry with extended beveled surfaces designed to shield noise from reaching the ground, also produce new noise sources due to scrubbing of the flow past structure, skin vibration, boundary layer noise, and edge noise due to the scattering of sound from sharp edges.

In 2010, a series of tests were initiated at NASA Glenn Research Center in order to study the propulsion/airframe integration. These experiements, under the umbrella of "Jet-Surface

Interaction Test (JSIT)," were intended to guide analytical studies towards prediction model development. The initial tests consisted of placement of a flat plate in the proximity of a round jet. Details of the experimental setup and test cofigurations are provided by C. Brown [Ref. 1], and G. Podboy [Ref. 2]. Measurements were gathered on both sides of the plate, commonly referred to as the reflected and shielded sides. In addition to the far-field microphone noise measurements [1], phased array source localization experiments [2] were carried out in order to shed light on the noise source location and its frequency content under different exhaust conditions.

An example of JSIT noise data that shows power specral density per Strouhal frequency in a 2-in diameter ($D$ =5.08cm) Mach 0.90 unheated jet, as reported by Brown in Ref. 1, is reproduced in figure 2. Here a solid surface extending 12-diameters from jet exit in the downstream direction was positioned at $D/2$ from the jet centerline. Far-field measurements are shown at 90° and at 100$D$ for a jet in isolation (no solid surface), as well as shielded and reflected sides of the jet in the presence of the surface.

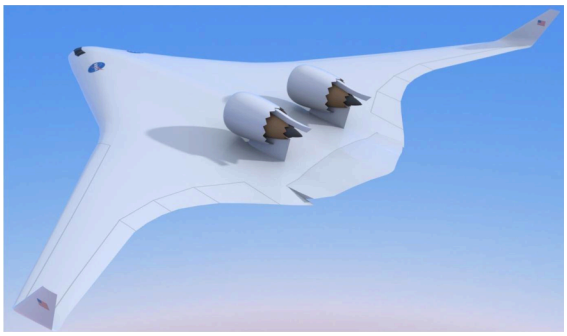

**Figure 1. Jet surface interaction.**

An extensive database has been generated as a function of the jet operating conditions and the length and position of the nearby solid surface. Similarly, an example of source localization data for the above jet is reported by Podboy as figure 17 of Ref. 2 (not shown here). It presents a beam-form map of the source location for an isolated jet as well as when surfaces of varying length are placed between jet and the phased array.

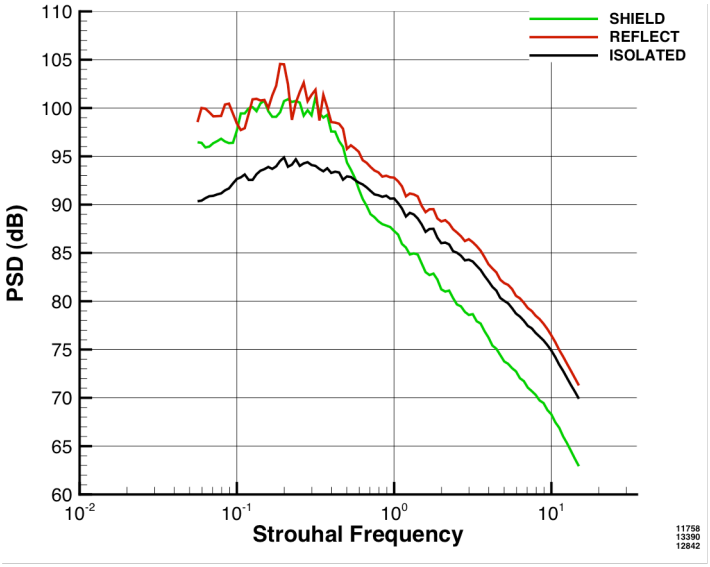


**Figure 2. Sample JSIT noise measurement as reported by C. Brown in Ref. 1.**

It is commonly accepted that the trailing edge noise is responsible for the enhanced low-frequency and peak noise amplitude measured on both reflected and shielded sides of the plate as seen in figure 2. A distinctive feature of the trailing edge noise component is its cardioid directivity shape and a dependence on jet velocity to the fifth power [Refs. 3, 4]. Recent measurements by Lawrence *et al*. [Ref. 5] indicate that the velocity power factor could be as large as 6 at longer plate length $L$ that yield a wetted trailing edge. FFowcs Williams and Hall [Ref. 3] describe a solution to the edge noise from a rigid plane in the presence of a turbulent flow using Lighthill's acoustic analogy. They

consider a very low Mach number flow, and take advantage of an appropriate Green's function applicable to a point source in the vicinity of a half-plane [Ref. 6]. Howe [Ref. 7] reviews various theoretical approaches in understanding the trailing-edge noise, and summarizes diverse theories into a single model that exhibits the dependence of the acoustic field on the turbulent fluctuations near the edge as well as the significance of the Kutta condition at this point. Goldstein [Ref. 8] includes the effect of the mean velocity gradient on the trailing edge noise by imposing a convecting vortex source, or gust, of the general form $\Omega(x_1/U(x_3)-t,x_2,x_3)$ on an incompressible transversely sheared mean flow.

Our interest here is the turbulence-generated noise due to the scrubbing of the jet flow past an adjacent flat surface. At very low Mach number, Howe [Ref. 9] describes the far field acoustic domain in terms of the wall-pressure wave number-frequency spectrum. Various models have been suggested for wall-pressure spectrum [Ref. 10] that are used in conjunction with a 2D or 3D free-space Green's function to express the far-field spectral density. These approximations ignore the mean flow refraction, compressibility effects, and sound produced outside the Boundary Layer (BL) at distances that are not small relative to the acoustic wavelength. At jet velocities of practical interest typical of a jet exhaust, frictional heat generation and thermal gradients in the BL could play important roles in generation as well as propagation of sound. Additionally, skin vibration could influence the surface boundary conditions and the subsequent radiated sound.

In section 2 we derive an expression for the propagation Green's function (GF) applicable to the scrubbing noise on a flat surface. The GF needs to be obtained numerically when the mean flow profiles are non-uniform. An expression for the far-field pressure is given in section 4. Ideally a RANS solution for the flow in the proximity of the surface provides the mean flow and turbulence information required in evaluating both the source strength and the GF. Sample GF computations using analytical profiles for the mean flow and a summary are provided in sections 6 and 7.

**2.0 Formulation of the Scrubbing Noise**

Consider turbulence-generated noise due to the scrubbing of a jet flow with an adjacent flat plane (Fig. 3). The mean flow is represented as a unidirectional transversely sheared flow (independent of $x_1$ and $x_2$ directions). We consider the mean static pressure $\bar{p}$ within the BL to be a constant. At very low Mach numbers the compressibility effects may be negligible, however at Mach numbers typical of a jet exhaust, frictional heat generation and thermal gradients in the BL could play important roles in generation as well as propagation of sound. The RANS solution provides such effects via the action of viscosity near the surface. Hence the noise generation process due to the scrubbing of a jet with a nearby surface is, in general, described by full acoustic analogy as considered in Appendix-A, and by Pridmore-Brown equation within a locally parallel flow approximation [Ref. 11]

$$L\pi' = \Gamma, \qquad \pi' \equiv \frac{p'(\vec{x},t)}{\gamma \bar{p}} \tag{1}$$

where $L$ is the operator

$$L \equiv D\left( D^2 - \frac{\partial}{\partial x_j}(c^2 \frac{\partial}{\partial x_j}) \right) + 2c^2 \frac{\partial U}{\partial x_j} \frac{\partial^2}{\partial x_1 \partial x_j}, \quad D \equiv \frac{\partial}{\partial t} + U \frac{\partial}{\partial x_1} \ , \tag{2}$$

and the source term $\Gamma(\vec{x},t)$ on the right hand side of (1) is defined according to the generalized acoustic analogy [Ref. 12]

$$\Gamma = \frac{1}{\gamma \bar{p}} \left( -D \frac{\partial}{\partial x_i}(c^2 \frac{\partial e_{ij}}{\partial x_j}) + 2c^2 \frac{\partial U}{\partial x_j} \frac{\partial^2 e_{ij}}{\partial x_1 \partial x_i} + D^2 Q \right) , \tag{3a}$$

$$Q = -(\gamma - 1)\left( \frac{1}{2} D(\rho v'^2) + \frac{\partial}{\partial x_j}(\rho v_j' h_o') + (\rho v_1' v_j') \frac{\partial U}{\partial x_j} \right) , \tag{3b}$$

stress tensor $e_{ij}$ is the difference between the fluctuating and Favre-averaged Reynolds stresses

$$e_{ij} = -(\rho v_i' v_j' - \overline{\rho v_i' v_j'}) , \tag{3c}$$

and $h_o'$ denotes the fluctuations in the moving-frame stagnation enthalpy (see the nomenclature).

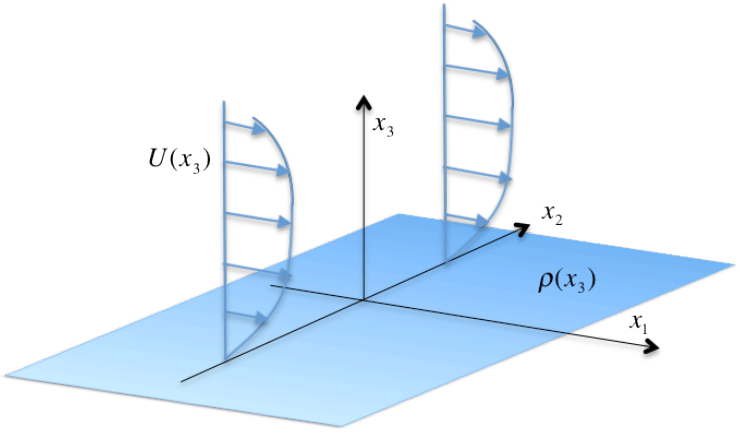


**Figure 3. Jet scrubbing on a nearby surface.**

The mean velocity $U$ and density $\bar{\rho}$ are functions of the normal coordinate ($x_3 > 0$), and $c$ is the mass-averaged speed of sound

$$U = U(x_3), \qquad c^2 = c^2(x_3) = \gamma \bar{p} / \bar{\rho}(x_3) . \tag{4}$$

Note that, in practice, both the mean flow and turbulence depend on the transverse direction $x_2$ as the source strength eventually diminishes at some distance $\pm L_2$ away from the jet centerline. In the stream-wise direction, the scrubbing effect may be limited to a distance $0 \le x_1 < L_1$, or the jet may persist beyond the plate edge at $L_1$ where interaction of the turbulence with the trailing edge produces edge noise. Here, in formulating the scrubbing noise problem, we limit the source to a

finite $x_2$ span by considering the mean flow as locally parallel in both $x_1$ and $x_2$ directions – thus express the problem in three dimensions. This assumption, although more suited to jets with a high aspect-ratio rectangular exhaust, permits source-volume integration within the wetted span in $x_2$ direction. A round jet may be transformed into a rectangular strip by using an appropriate conformal mapping transformation. When all changes in span-wise $x_2$ direction are neglected, the sound intensity should be expressed as per unit thickness. The special 2D case will be discussed in section 5.

We seek a solution to equation (1) of the form

$$\pi'(\vec{x},t) = \int_{\vec{y}} \int_{\tau} G(\vec{x},t;\vec{y},\tau)\Gamma(\vec{y},\tau)d\tau d\vec{y} \ , \tag{5}$$

where $G$ denotes the GF

$$LG(\vec{x},t;\vec{y},\tau) = \delta(\vec{x}-\vec{y})\delta(t-\tau) \ . \tag{6}$$

In a bounded media, the above form of the solution requires for the GF to satisfy certain boundary conditions on the plate. The source-volume integration in (5) is carried out over noise-generating region $\vec{y}$ in the vicinity of the scrubbing surface and at the emission time $\tau$. The solution described in the following excludes the trailing edge noise that travels to the opposite side of the surface as alluded to earlier. This latter noise component requires a Wiener-Hopf type solution.

We define a Fourier Transform (FT) pair with respect to $(x_1,x_2)$ coordinates as well as time $t$. The corresponding wave number vector is denoted as $\vec{k}_t = (k_1,k_2)$

$$\begin{aligned}
\hat{G}(\vec{k}_t,x_3,y_3,\omega) &= \frac{1}{(2\pi)^3}\int_{-\infty}^{\infty}\int_{-\infty}^{\infty}\int_{-\infty}^{\infty} G(\vec{x},t;\vec{y},\tau)e^{-i[k_1(x_1-y_1)+k_2(x_2-y_2)-\omega(t-\tau)]}d(x_1-y_1)d(x_2-y_2)d(t-\tau) \\
G(\vec{x},t;\vec{y},\tau) &= \int_{-\infty}^{\infty}\int_{-\infty}^{\infty}\int_{-\infty}^{\infty} \hat{G}(\vec{k}_t,x_3,y_3,\omega)e^{i[k_1(x_1-y_1)+k_2(x_2-y_2)-\omega(t-\tau)]}dk_1dk_2d\omega \ .
\end{aligned} \tag{7}$$

Throughout, an over hat carrot is used to denote a FT variable as defined above.

The transform of equation (6) is

$$\frac{\partial^2\hat{G}}{\partial x_3^2} + \left(\frac{(c^2)'}{c^2} - \frac{2k_1U'}{-\omega+k_1U}\right)\frac{\partial\hat{G}}{\partial x_3} + \left(\frac{(-\omega+k_1U)^2}{c^2} - k_1^2 - k_2^2\right)\hat{G} = \frac{i}{(2\pi)^3}\frac{\delta(x_3-y_3)}{c^2(-\omega+k_1U)} \ , \tag{8}$$

where prime as used on mean variables $c^2$ and $U$ denotes differentiation with respect to $x_3$. The equation possesses a critical layer at $x_3$ where factor $-\omega+k_1U(x_3)$ vanishes. To avoid this

singularity we require $k_1 < \omega / U_e$ where $U_e$ denotes some peak mean velocity in the BL. This upper limit for $k_1$ is usually referred to as the non-convective domain for the wave number. As discussed in [Refs. 13, 14], in the convective domain $k_1 > \omega / U_e$ it becomes necessary to provide a loss mechanism, such as turbulent viscosity, in order to evade the singularity. The dominant value of $k_1$ contributing to the far-field noise will be determined in section 3. It will be shown that when $U_e < c_\infty$ the upper limit condition stated for $k_1$ will be satisfied at all observer location.

For convenience, the second-order linear differential equation (8) is rearranged as

$$\frac{\partial^2 \breve{G}}{\partial x_3^2} + f(\vec{k}_t, x_3, \omega)\breve{G} = \delta(x_3 - y_3) \ . \tag{9}$$

Since equation (9) is self-adjoint, the newly defined GF, $\breve{G}$, is symmetric in ($x_3$, $y_3$), i.e., $\breve{G}(\vec{k}_t, x_3, y_3, \omega) = \breve{G}(\vec{k}_t, y_3, x_3, \omega)$ and is related to the GF of interest $\hat{G}$ as

$$\hat{G}(\vec{k}_t, x_3, y_3, \omega) = \frac{i}{(2\pi)^3} \frac{1}{c(y_3)c(x_3)} \frac{-\omega + k_1 U(x_3)}{\left(-\omega + k_1 U(y_3)\right)^2} \breve{G}(\vec{k}_t, x_3, y_3, \omega) \ , \tag{10}$$

where

$$\begin{aligned} f(\vec{k}_t, x_3, \omega) &= \chi^2 - \mathbb{C}^2 - \frac{2(k_1 U')^2}{(-\omega + k_1 U)^2} + \frac{k_1 U''}{-\omega + k_1 U} + \frac{(c^2)'}{c^2} \frac{k_1 U'}{-\omega + k_1 U} \ , \\ \chi^2(\vec{k}_t, x_3, \omega) &= \frac{(-\omega + k_1 U)^2}{c^2} - k_1^2 - k_2^2 \, , \\ \mathbb{C}^2(x_3) &= \frac{1}{2} \frac{\partial}{\partial x_3} \left( \frac{(c^2)'}{c^2} \right) + \frac{1}{4} \left( \frac{(c^2)'}{c^2} \right)^2 . \end{aligned} \tag{11}$$

and $(c^2)' / c^2 = (\partial \overline{\rho} / \partial x_3) / \overline{\rho}$.

It should be noted that unlike the present problem, the propagation equation might not, in general, reduce to a self-adjoint from. Such is the case when the governing equations are written for a spreading flow [Ref. 15]. In that case, working with the adjoint GF will entail additional integrals that should be carried out on the surfaces. A general solution for the five field variables using a vector GF formulation is provided in Appendix A. The second integral in equation (A16) in the appendix describes the contribution to the acoustic field due to the nearby surfaces. In the formulation described herein, the GF satisfies conditions that make the surface integral equal to zero.

Far away from the noise generating region, as $x_3 \to \infty$ the mean velocity and the sound speed approach their respective ambient values $U_\infty$ and $c_\infty$, and equations (9) and (11) show that

$$\frac{\partial^2 \breve{G}}{\partial^2 x_3^2} + \chi_\infty^2 \breve{G} = 0, \quad x_3 \to \infty \tag{12a}$$

where

$$\chi_\infty^2 = (-\kappa_o + k_1 M_\infty)^2 - k_1^2 - k_2^2 \; ; \quad \kappa_o = \omega / c_\infty \; , \quad M_\infty = U_\infty / c_\infty \tag{12b}$$

The Mach number $M_\infty$ takes account of the flight effect when surface is in motion relative to the ambient. The far-field solution to equation (12a) is

$$\breve{G}(\vec{k}_t, x_3, y_3, \omega) = b \, e^{-i\chi_\infty x_3}, \quad x_3 \to \infty \tag{13a}$$

where complex number $b$ has dimension of length, and in general depends on $\omega, k_1, k_2$. An outgoing propagating wave requires the negative root of $\chi_\infty^2$ when $\chi_\infty^2 > 0$, and when $\chi_\infty^2$ is negative the branch-cut is chosen such that $\chi_\infty = -i(|\chi_\infty^2|)^{1/2}$. When $\chi_\infty^2 < 0$ the pressure decays exponentially normal to the surface (evanescent waves). Aerodynamic noise scattered off the edge of a half-plane is sometimes described [Ref. 16, 17] as the interaction of evanescent waves (rather than propagating acoustic waves) with the edge. These disturbances are dominated by spectral components that possess a subsonic phase velocity in a constant $x_3$ plane.

Since we are interested in the scrubbing noise that reaches a distant observer, the radiation field would be dominated by wave numbers, in constant $x_3$ plane, that possess a supersonic phase velocity

$$\frac{\omega}{M_\infty k_1 + \sqrt{k_1^2 + k_2^2}} > c_\infty \tag{13b}$$

The far-field boundary condition for a bounded solution to equation (9) requires

$$\frac{\partial \breve{G}}{\partial x_3} + i\chi_\infty \breve{G} = 0, \quad x_3 \to \infty \; , \tag{14}$$

and a no slip boundary condition on the scrubbing surface ($U = 0, x_3 \to 0$) combined with the $x_3$ component of the linearized momentum equation within the turbulent boundary layer (TBL) shows that

$$\frac{\partial(\rho v_3')}{\partial t} + \frac{\partial p'}{\partial x_3} = 0, \qquad x_3 \to 0 \tag{15}$$

Upon replacing $\rho$ with the mean fluid density $\rho_o$ near the surface, we apply a FT to the latter equation to obtain

$$-i\omega\rho_o \widehat{v_3'} + \frac{\partial \widehat{p'}}{\partial x_3} = 0, \qquad x_3 \to 0 \tag{16}$$

Assuming that Fourier components of the normal velocity and pressure on the surface relate through the surface impedance $Z(\omega)$ as

$$\widehat{p'} = Z\,\widehat{v_3'}\,, \qquad x_3 = 0 \tag{17}$$

we find

$$\frac{\partial \widehat{\pi'}}{\partial x_3} - \frac{i\rho_o\omega}{Z}\widehat{\pi'} = 0, \qquad x_3 = 0\ . \tag{18}$$

Since the FT of a convolution is the product of the Fourier transforms, equations (5) implies

$$\widehat{\pi'}(\vec{k}_t, x_3, \omega) = (2\pi)^3 \int_{y_3} \hat{G}(\vec{k}_t, x_3, y_3, \omega)\hat{\Gamma}(\vec{k}_t, y_3, \omega)\,dy_3\ , \tag{19}$$

and upon using (19) in (18) we find

$$\frac{\partial \hat{G}}{\partial x_3} - \frac{i\rho_o\omega}{Z}\hat{G} = 0, \qquad x_3 = 0 \tag{20}$$

Our interest is in the boundary condition applicable to $\breve{G}$ rather than $\hat{G}$. Substituting equation (10) in (20) shows that

$$\frac{\partial \breve{G}}{\partial x_3} - \psi\breve{G} = 0\,, \qquad x_3 = 0 \tag{21a}$$

$$\psi(k_1, \omega, \overline{Z}) = \left( \frac{i\kappa_o}{\overline{Z}} \frac{c_\infty^2}{c_o^2} + \frac{c_o'}{c_o} + \frac{k_1}{\omega} U'(0) \right), \quad \overline{Z}(\omega) \equiv \frac{Z(\omega)}{\rho_\infty c_\infty} \tag{21b}$$

where $c_o$ is the mean sound speed in the fluid at the surface interface, and $c_o'$ is its derivative at $x_3$ = 0. An alternative way of deriving the surface boundary condition (21a) is described in Appendix B.

The problem at hand is thus reduced to solving equation (9) subject to the two boundary conditions (14) and (21).

The two boundary conditions could be expressed in a more general form as

$$\alpha_i \frac{\partial \widehat{\pi'}}{\partial x_3} + \beta_i \widehat{\pi'} = \gamma_i\ , \qquad i = 1,2 \tag{22}$$

where *i*=1 and 2 refer to the boundary points at $x_3$ = 0 and ∞. A non-zero value of $\gamma_i$ (such as presence of a source term in the linearized momentum equation near the surface) would contribute to the homogeneous solution to the differential equation. However, for our problem we consider $\gamma_1 = \gamma_2 = 0$, thus the homogeneous solution is identically zero, and we are left with the particular solution only.

The GF in equation (9) may be expressed in terms of two linearly independent solutions $V_i(\vec{k}_t, x_3, \omega)$ to the homogeneous equation

$$\partial^2 V_i / \partial x_3^2 + f V_i = 0, \qquad i = 1,2 \tag{23a}$$

such that $V_1$ and $V_2$ satisfy the homogeneous boundary conditions at 0 and $\infty$, respectively. For brevity we omit $\vec{k}_t$ and $\omega$ from the arguments of $V_1$ and $V_2$.

$$\frac{\partial V_1(x_3)}{\partial x_3} - \psi V_1(x_3) = 0, \quad x_3 = 0 \tag{23b}$$

$$\frac{\partial V_2(x_3)}{\partial x_3} + i\chi_\infty V_2 = 0, \quad x_3 \to \infty \tag{23c}$$

and

$$\breve{G}(\vec{k}_t, x_3, y_3, \omega) = \begin{cases} V_2(x_3)V_1(y_3)/W(y_3), & y_3 < x_3 \\ V_1(x_3)V_2(y_3)/W(y_3), & y_3 > x_3 \end{cases} \tag{24}$$

and $W\left(V_1, V_2(y_3)\right)$ is the Wronskian. For convenience we normalize both $V_1$ and $V_2$ at zero argument $y_3 = 0$ such that

$$V_1(0) = V_2(0) = 1, \tag{25}$$

and since according to Abel's formula the Wronskian to equation (23a) is independent of $y_3$, then we evaluate $W = W_o$ at the surface. Equations (23b,c) and (25) conclude that

$$W_o(\vec{k}_t, \omega, \overline{Z}) = V_2'(0) - \psi(k_1, \omega, \overline{Z}). \tag{26}$$

The above expression shows that the Wronskian $W_o$ depends on the BL velocity and temperature profiles at $y_3 = 0$, as well as the surface impedance $\overline{Z}$ through parameter $\psi$. It is noted that equation (23a) supports Helmholtz instabilities that would arise when $\vec{k}_t$ and $\omega$ satisfy the Eigen-wave condition $W_o(\vec{k}_t, \omega, \overline{Z}) = 0$. The instability waves could be triggered when the BL profile supports the Eigen-wave condition. These waves could grow exponentially and dominate the region they occupy. Subsequently we need to set the wave number limit to avoid these special cases. For example, when the surface is rigid and the BL is considered as incompressible such that $\psi(k_1, \omega, \overline{Z}) = k_1 U'(0)/\omega$, we should require $V_2'(0)/U'(0) > 1/U_e$ for the Wronskian $W_o$ to remain non-zero for all wave numbers within the non-convective range $k_1 < \omega / U_e$. However as we will discuss shortly, $V_2'(0)$ is not known a priori and is determined only after equation (20a) is solved as a boundary value problem. Jones [Ref. 18] studied the instability of a two-dimensional shear layer using a model velocity profile in which the velocity increased linearly from 0 to $U_e$ over a distance of *h* from the surface and then remained constant. He showed that

the onset of Helmholtz instabilities occur at a Strouhal frequency of $\omega h / U_e \sim 1/3$ where $\omega$ denotes the frequency of sound waves falling on the shear layer. At frequencies above this critical value the layer remained stable.

Upon placing (24) into (10), the Fourier transformed GF at an observer point above the source region is given as

$$\hat{G}(\vec{k}_t, x_3, y_3, \omega) = \frac{i}{(2\pi)^3} \frac{1}{c(y_3)c(x_3)} \frac{-\omega + k_1 U(x_3)}{\left(-\omega + k_1 U(y_3)\right)^2} \frac{V_2(x_3) V_1(y_3)}{W_o}, \quad x_3 > y_3 \tag{27}$$

An alternative form of the GF valid for $x_3 < y_3$ (see equation 24) should be used if one were interested in the surface pressure. The two functions $V_i$ are determined numerically. The first variable is evaluated when equation (23a) is solved as an initial value problem with $V_1(0) = 1$ and $V_1'(0) = \psi$. The second variable is determined when (23a) is solved as a boundary value problem subject to $V_2(0) = 1$, and $V_2'(x_3) + i\chi V_2(x_3) = 0$ as $x_3 \to \infty$. Fortunately, as we shall see next, there are only certain values of wave numbers $k_1$ and $k_2$ that make the major contribution to the radiated far-field noise.

**3.0 Stationary Phase Method**

We apply an inverse FT with respect to wave numbers $k_1$ and $k_2$ and write the GF as

$$\mathbf{G}(\vec{x}, \vec{y}; \omega) = \int_{-\infty}^{\infty} \int_{-\infty}^{\infty} \hat{G}(\vec{k}_t, x_3, y_3, \omega) e^{i[k_1(x_1 - y_1) + k_2(x_2 - y_2)]} dk_1 dk_2 \ . \tag{28}$$

Since the interest is in the far-field noise, the appropriate from for $V_2$ is

$$V_2(\vec{k}_t, x_3, \omega) = b_2 e^{-i\chi_\infty x_3}, \qquad x_3 \to \infty \ . \tag{29}$$

Complex number $b_2(\vec{k}_t, \omega)$ has a dimension of unity, and should be a known parameter once the boundary value problem (23a) is solved for $V_2$. Placing (27) and (29) into (28), the double integral involving wave numbers $k_1$ and $k_2$ becomes

$$\mathbf{G}(\vec{x}, \vec{y}; \omega) = \frac{i}{(2\pi)^3} \frac{1}{c(y_3)c(x_3)} \iint_{k_1 k_2} \frac{-\omega + k_1 U(x_3)}{\left(-\omega + k_1 U(y_3)\right)^2} \frac{b_2 V_1(\vec{k}_t, y_3, \omega)}{W_o(\vec{k}_t, \omega, \bar{Z})} e^{i\Theta(\vec{k}_t, \vec{x}, \omega)} dk_1 dk_2 \ , \tag{30}$$

where

$$\Theta(\vec{k}_t, \vec{x}, \omega) = k_1(x_1 - y_1) + k_2(x_2 - y_2) - \chi_\infty x_3 \ . \tag{31}$$

We adopt a spherical coordinate system where $\theta$ is the angle the observer position vector makes with the direction of the mean flow (Fig. 4)

$$(x_1 - y_1, x_2 - y_2, x_3) = R(\sin\phi\cos\theta,\ \cos\phi,\ \sin\phi\sin\theta), \quad x_3 \to \infty \ , \tag{32}$$

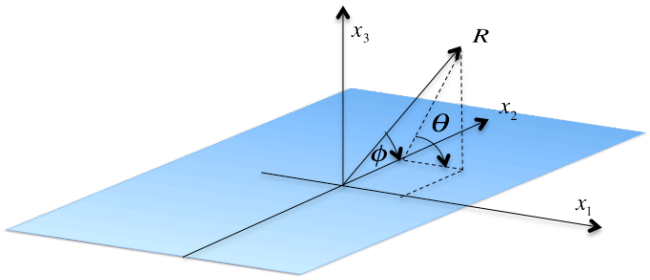


**Figure 4. Spherical coordinates** $0 \le \theta \le \pi,\ 0 \le \phi \le \pi$.

where $R = |\vec{x} - \vec{y}|$. The wave number vector in expressed in a similar fashion as

$$(k_1, k_2, k_3) = \kappa_o(\sin\phi'\cos\theta',\ \cos\phi',\ \sin\phi'\sin\theta') \ . \tag{33}$$

Using (32) and (33) in (31), and upon neglecting the flight effect, the phase factor becomes

$$\Theta(\vec{k}_t, \vec{x}, \omega) = R\kappa_o\left(\sin\phi\sin\phi'\cos(\theta - \theta') + \cos\phi\cos\phi'\right), \quad M_\infty = 0 \ , \tag{34}$$

where we have selected $\chi_\infty = -\kappa_o \sin\phi'\sin\theta'$. The large parameter in applying the stationary phase technique [Ref. 19] is $R\kappa_o \gg 1$. This requires the source to observer distance $R$ to be much larger than the wavelength of the radiated sound. If we define a Strouhal frequency as $St = \omega\delta_o / U_e$, where $\delta_o$ is the BL thickness (distance from the wall at which the mean velocity is $0.99U_e$), then the large parameter requirement implies $St >> c_\infty \delta_o / (U_e R)$ which is not a very stringent condition even at relatively low frequency.

The Jacobian in making coordinates transformation from $(k_1, k_2)$ to $(\theta', \phi')$ is $\kappa_o^2 \sin\theta' \sin^2\phi'$ or $dk_1 dk_2 = \kappa_o^2 \sin\theta' \sin^2\phi' d\theta' d\phi'$.

Using the new coordinates, the point of stationary phase $(\theta^*, \phi^*)$ is obtained when we set equal to zero the two partial derivatives of phase factor $\Theta$.

$$\frac{\partial\Theta}{\partial\theta'} = 0, \quad \frac{\partial\Theta}{\partial\phi'} = 0 \ . \tag{35}$$

which results in

$$\theta^* = \theta, \quad \phi^* = \phi \, . \tag{36}$$

Equation (36) simply implies that in the absence of flight effect, the major contribution to the radiated sound field is due to wave numbers with magnitude $\kappa_o$ in the same direction as the observer point $(\theta,\phi)$. Subsequently the contribution to the integral in (30) in the vicinity of the stationary point is obtained when we expand the phase $\Theta$ (to second order) about this point, and evaluate the rest of the integrand at the point of stationary phase $\vec{k}_t^{\bullet} = (k_1^{\bullet}, k_2^{\bullet})$.

$$\begin{aligned}
&\vec{k}_t^{\bullet} = \kappa_o(\sin\phi\cos\theta,\ \cos\phi),\\
&\mathbf{G}(\vec{x},\vec{y};\omega) \sim \frac{i}{(2\pi)^3}\frac{-\omega}{\left(-\omega + k_1^{\bullet}U(y_3)\right)^2}\frac{b_2(\vec{k}_t^{\bullet},\omega)V_1(\vec{k}_t^{\bullet},y_3,\omega)}{c_\infty c(y_3)W_o\left(k_1^{\bullet},\omega,\bar{Z}\right)}\times\\
&\quad\int_{\theta'}\int_{\phi'}\exp\left(i\kappa_o R\left\{1-\frac{1}{2}(\theta'-\theta)^2\sin^2\phi-\frac{1}{2}(\phi'-\phi)^2\right\}\right)(\kappa_o^2\sin\theta\sin^2\phi\, d\theta' d\phi'),
\end{aligned} \tag{37}$$

as $(R\to\infty)$. The above double integral is now evaluated as

$$e^{i\kappa_o R}\kappa_o^2\sin\theta\sin^2\phi\int_{-\infty}^{\infty}\int_{-\infty}^{\infty}\exp\left(-\frac{i\kappa_o R}{2}(\alpha^2\sin^2\phi+\beta^2)\right)d\alpha d\beta = -2\pi i\kappa_o\frac{\sin\theta\sin\phi}{R}e^{i\kappa_o R}\ . \tag{38}$$

Placing this result back in (37) shows

$$\mathbf{G}(\vec{x},\vec{y};\omega)\sim -\frac{1}{(2\pi)^2}\frac{e^{i\kappa_o R}}{R}\frac{\sin\theta\sin\phi}{c_\infty^2 c(y_3)}\frac{b_2(\vec{k}_t^{\bullet},\omega)V_1(\vec{k}_t^{\bullet},y_3,\omega)}{W_o\left(\vec{k}_t^{\bullet},\omega,\bar{Z}\right)}\frac{1}{\left(1-\sin\phi\cos\theta\dfrac{U(y_3)}{c_\infty}\right)^2}\ . \tag{39}$$

The GF $G(\vec{x},t;\vec{y},\tau)$ is now obtained as

$$G(\vec{x},t;\vec{y},\tau) = \int_{-\infty}^{\infty}\mathbf{G}(\vec{x},\vec{y};\omega)e^{-i\omega(t-\tau)}d\omega\ . \tag{40}$$

Note that with $k_1 = \kappa_o\sin\phi\cos\theta$, the upper limit placed on $k_1$ in section 2 will be satisfied at all subsonic conditions $U_j/c_\infty < 1$. At supersonic conditions only certain observer locations will be subject to the critical layer singularity.

## 4.0 Far-Field Acoustics

The far-field sound spectral density is evaluated as a FT of the pressure auto-covariance

$$\overline{p^2}(\vec{x},\omega) = (\gamma\bar{p})^2\int_{-\infty}^{\infty}e^{i\omega\tau}\left[\frac{1}{2T}\int_{-T}^{T}\pi'(\vec{x},t)\pi'(\vec{x},t+\tau)dt\right]d\tau\ . \tag{41}$$

where $T$ denotes some large time. Upon placing (5) and (40) into (41), it is shown that [Ref. 20]

$$\overline{p^2}(\vec{x},\omega)=\int_{\vec{y}}\int_{\vec{\xi}}\int_{\tau=-\infty}^{\infty}\mathbf{G}^*(\vec{x},\vec{y}-\vec{\xi}/2,\omega)\mathbf{G}(\vec{x},\vec{y}+\vec{\xi}/2,\omega)q(\vec{y},\vec{\xi},\tau)e^{i\omega t}d\tau d\vec{\xi}d\vec{y}\ , \tag{42}$$

where $q$ denotes a two-point space-time correlation between noise generating sources at points A and B separated by space $\vec{\xi}$ and time $\tau$. Using the source term in equation (1) we have

$$q(\vec{y},\vec{\xi},\tau)=(\gamma\overline{p})^2\lim_{T\to\infty}\frac{1}{2T}\int_{-T}^{T}\Gamma^*(\vec{y}-\vec{\xi}/2,t)\Gamma(\vec{y}+\vec{\xi}/2,t+\tau)dt\ . \tag{43}$$

Since the exponential phase factor in the GF equation (39) depends on the distance $R=|\vec{x}-\vec{y}|$ between observer point $\vec{x}$ and source point $\vec{y}$, the product of the GF and its conjugate (denoted by *) is evaluated at the center of the correlation multiplied by a phase factor $\exp(-i\vec{k}.\vec{\xi})$, where wave number $\vec{k}$ is directed as $\vec{x}-\vec{y}$ and has a magnitude of $\kappa_o$

$$\overline{p^2}(\vec{x},\omega)=\int_{\vec{y}}|\mathbf{G}(\vec{x},\vec{y};\omega)|^2\int_{\vec{\xi}}\int_{\tau=-\infty}^{\infty}q(\vec{y},\vec{\xi},\tau)e^{i\omega\tau-i\vec{k}.\vec{\xi}}d\tau d\vec{\xi}d\vec{y}\ . \tag{44}$$

As is a common practice in acoustic analogy noise-prediction models, the space-time FT of the source correlation function, denoted as the inner double integral in (44), is evaluated in closed-form once an acceptable physics-based source model is obtained. The modeling becomes much less cumbersome if the spatial derivatives present in the source were to be transferred to the GF within equation (5) and prior to forming the sound spectral density function. Subsequently, the final GF as defined in (39) could be subject to new spatial derivatives at the source point $\vec{y}$ while source $\Gamma(\vec{y},t)$ would be free of similar derivatives.

Since the GF depends on both $V_1$ and $V_2$, which in turn depend on $\omega$, $\theta$, and $\phi$, the pair $(V_1,V_2)$ is determined numerically per pre-selected observer angles and frequency using the local BL mean velocity and density profiles. The integral over the source region in equation (44) is then evaluated to obtain the far-field noise as a contribution from independent correlation volume elements that comprise the source. As pointed out earlier, the volume integration is limited to regions with relatively stronger source strength while the mean flow is considered as locally parallel in both $x_1$ and $x_2$ directions.

In the limit of very low Mach number ($M<0.10$), it is argued [Ref. 9] that there is a direct correspondence between the acoustic domain of the wall-pressure spectrum and the far-field spectral density of the radiated sound. This approximation ignores mean flow refraction and sound produced by the turbulence outside the boundary layer at distances that are not small relative to the acoustic wavelength. Following this argument, at large distance $R$ from a hard wall region of area $A$, Howe [Ref. 21] proposed an expression for the sound spectral density in terms of the so-called blocked pressure, which in the present notation is

$$\overline{p^2}(\vec{x},\omega)=A\kappa_o^2\frac{\sin^2\theta\sin^2\phi}{R^2}P(\vec{k}_t,\omega)\ , \tag{45}$$

where $P(\vec{k}_t,\omega)$ is the wall-pressure wave number-frequency spectrum, and is defined as a FT of the space-time pressure correlation function $q(\xi_1,\xi_2,\tau)$ of the wall-pressure

$$P(\vec{k}_t,\omega)=\frac{1}{(2\pi)^3}\int_{\tau=-\infty}^{\infty}\int_{A} q(\xi_1,\xi_2,\tau)\exp\left(i\omega\tau-i\vec{k}_t.\vec{\xi}_t\right)d\tau d\xi_1 d\xi_2 \ . \tag{46}$$

Here $\vec{\xi}_t$ is the spatial separation vector of the correlation on the surface and $\vec{k}_t$ is the corresponding wave-number vector. The wall-pressure correlation function over a rectangular area *A* is defined as

$$q(\xi_1,\xi_2,\tau)=\lim_{T\to\infty}\frac{1}{2T}\frac{1}{A}\int_{-T}^{T}\int_{-L_1}^{L_1}\int_{-L_2}^{L_2} p'(y_1,y_2,0,t)p'(y_1+\xi_1,y_2+\xi_2,0,t+\tau)dy_1dy_2dt \ . \tag{47}$$

Various models for $P(\vec{k}_t,\omega)$ have been proposed in the literature, however there is no universally accepted form for the wall-pressure spectrum that could directly be substituted into (45). For example low wave number measurements of Sevik [Ref. 10] suggest

$$\frac{P(\vec{k}_t,\omega)}{\rho_\infty^2 v_*^3\delta_o^3}\approx\frac{127(U_e/c_\infty)^2(v_*/U_e)}{(\omega\delta_o/U_e)^{4.5}},\quad 24<\frac{\omega\delta_o}{U_e}<240,\quad 0.01<\frac{U_e}{c_\infty}<0.15. \tag{48}$$

where $v_*\approx 0.03U_e$ is the friction velocity, and $\delta_o$ denotes the BL thickness as defined earlier.

More complicated expressions have been suggested for the wall-pressure wave number-frequency spectrum $P(\vec{k}_t,\omega)$ with additional parameters that are meant to account for the attenuation and refraction of sound in the BL [Ref. 22] and/or surface roughness [Ref. 23] and dependence on the individual wave number components on the surface. The validity of these empirical models remains to be confirmed experimentally. A comparison of semi-empirical equation (45) with the analytical solution given in equation (44) shows that the latter should account for all of the above-mentioned effects when source information as well as the GF are available within and outside the BL. Ideally, a RANS solution to the wall-bounded flow would provide both the mean flow and turbulence information required in evaluating the GF and the source correlation in a turbulent boundary layer and the main jet.

## 5.0 Two-Dimensional Approximation

When mean flow and turbulence are independent of the transverse direction $x_2$ (unlike in section 3 where the rectangular flow was limited to a finite $x_2$ domain), the analysis is carried out in two dimensions. Following the steps outlined earlier, the new GF is obtained from an equation similar to (30)

$$\mathbf{G}(\vec{x},\vec{y};\omega)=\frac{i}{(2\pi)^2}\frac{1}{c(y_3)c(x_3)}\int_{k_1}\frac{-\omega+k_1U(x_3)}{\left(-\omega+k_1U(y_3)\right)^2}\frac{b_2V_1(k_1,y_3,\omega)}{W_o(k_1,\omega,\bar{Z})}e^{i\Theta(k_1,\vec{x},\omega)}dk_1 \ , \tag{49}$$

where phase parameter is now defined as

$$\Theta(k_1,\vec{x},\omega) = k_1(x_1 - y_1) - \chi_\infty x_3\,, \quad \chi_\infty^2 = \kappa_o^2 - k_1^2\,. \tag{50}$$

It is readily shown that the point of stationary phase is $k_1^{\bullet} = \kappa_o \cos\theta$, and

$$\mathbf{G}(\vec{x},\vec{y};\omega) \sim -\frac{e^{i\pi/4}}{(2\pi)^{3/2}} \frac{e^{i\kappa_o R}}{\sqrt{\kappa_o R}} \frac{\sin\theta}{c_\infty^2 c(y_3)} \frac{b_2(k_1^{\bullet},\omega) V_1(k_1^{\bullet},y_3,\omega)}{W_o\left(k_1^{\bullet},\omega,\bar{Z}\right)} \frac{1}{(1-\frac{U(y_3)}{c_\infty}\cos\theta)^2}\,. \tag{51}$$

The source correlation now uses $\vec{\xi} = (\xi_1,\xi_3)$ as a separation vector, and the far-field sound is evaluated using equation (42) with the volume element as $d\vec{y} = dy_1 dy_3$, and per unit flow thickness in $x_2$ direction. Note that both 3D and 2D expressions for the GF could be written in a similar from if equations (39) and (51) were normalized with respect to their corresponding free-space GF.

## 6.0 Numerical Results

Sample Green's function calculations are presented using analytical representations of the jet mean velocity and temperature profiles in the proximity of a flat surface.

The mean velocity profile adopted here depends on the normal direction $y_3$ only, and is modeled for a jet with thickness $D_j = 2$ in

$$\frac{U(\eta)}{U_j} = \begin{cases} \tanh(\dfrac{D_j\eta}{d_1}), & \eta < 1.05 \\ \dfrac{1}{2} + \dfrac{1}{2}\tanh\dfrac{1}{d_2}\left(\dfrac{1/2}{\eta-1} - \dfrac{\eta-1}{1/2}\right), & \eta \geq 1.05 \end{cases} \tag{52}$$

Using parameters $(d_1, d_2) = (0.10, 2.0)$, the velocity profile, divided by jet velocity $U_j$, is plotted (Fig. 5) as a function of the non-dimensional distance from the wall $\eta = y_3 / D_j$. The boundary layer thickness for this flow is $\delta_o / D_j = 1.324 d_1$.

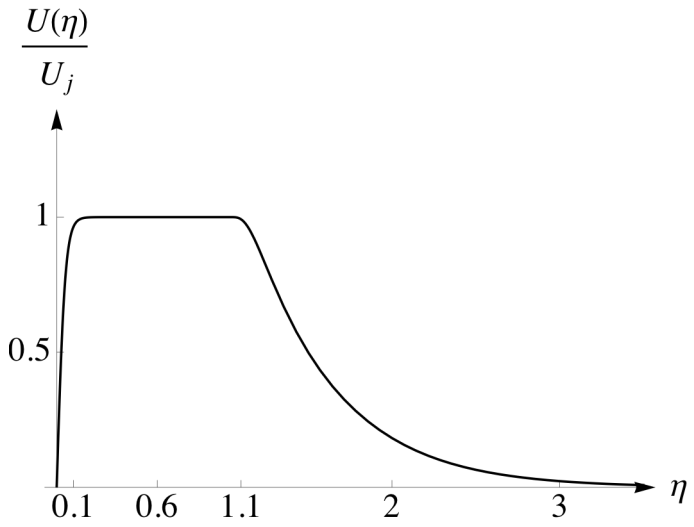


**Figure 5. Mean velocity profile.**

The mean static temperature is modeled as a composite of the two profiles – the first is obtained by placing the above velocity profile in Crocco-Busemann law

$$\frac{T_1(\eta)}{T_\infty} = 1 + (T_R - 1)\frac{U(\eta)}{U_j} - \frac{\gamma - 1}{2}\left(\frac{U(\eta)}{c_\infty}\right)^2, \tag{53a}$$

where $T_R$ is the jet plenum stagnation temperature ratio. The second profile is intended to simulate frictional heat generation in the proximity of the wall

$$\frac{T_2(\eta)}{T_\infty} = \frac{1}{d_3}\left(\frac{1}{2} + \frac{1}{2}\tanh\frac{1}{d_4}\left(\frac{1}{D_j\eta} - D_j\eta\right)\right). \tag{53b}$$

Using parameters $(d_3, d_4) = (4.0, 3.0)$ the temperature profile $T(\eta) = T_1(\eta) + T_2(\eta)$ is shown in Fig. 6 subject to jet exit values of $U_j / c_\infty = 0.90$, and $T_R = 3.0$. The ideal gas law $c^2 = \gamma \Re T$ was used to construct the speed of sound as shown in Fig. 6.

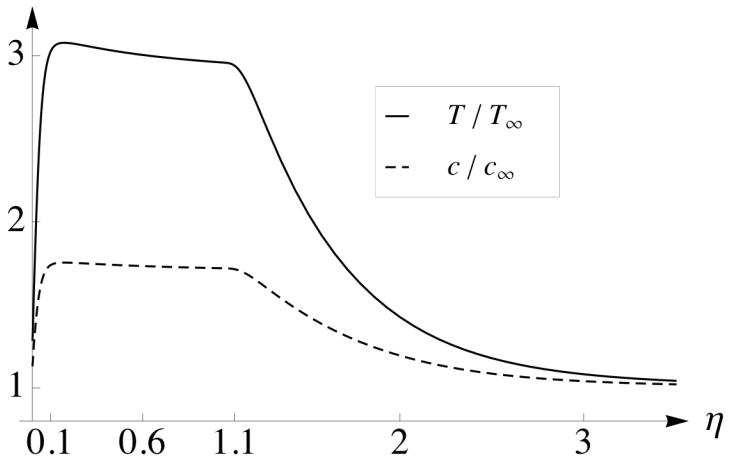


**Figure 6. Mean profiles for static temperature (solid line) and sound speed (dashed line) at $T_R = 3.0$ .**

The GF is solved numerically at specific values of the Strouhal frequency $St_o$ defined as

$$St_o \equiv \frac{1}{2\pi}\frac{\omega D_j}{U_j} \ , \tag{54}$$

We define non-dimensional parameters $\bar{\kappa} = \kappa_o D_j = 2\pi\, St_o (U_j / c_\infty)$ , $\bar{c} = c / c_\infty$ , $\bar{U} = U / c_\infty$ , $\bar{R} = R / D_j$ , and divide the 3D and 2D expressions in (39) and (51) by their respective free-space values of $(-e^{i\bar{\kappa}\bar{R}} / 4\pi\bar{R})$ and $(-e^{i\bar{\kappa}\bar{R}+i\pi/4} / \sqrt{8\pi\bar{\kappa}\bar{R}}\,)$. Additionally constant $1/(\pi c_\infty^3)$ is factored out in order to define a normalized GF applicable to the far field

$$G_N(\eta,\omega) = \left| \begin{array}{ll} \dfrac{\sin\theta\sin\phi}{\bar{c}}\dfrac{b_2(\vec{k}_t^{\,*},\omega)V_1(\vec{k}_t^{\,*},\eta,\omega)}{\bar{W}_o(\vec{k}_t^{\,*},\omega,\bar{Z})}\dfrac{1}{(1-\bar{U}\sin\phi\cos\theta)^2}, & \text{3D} \\ \dfrac{\sin\theta}{\bar{c}}\dfrac{b_2(k_1^*,\omega)V_1(k_1^*,\eta,\omega)}{\bar{W}_o(k_1^*,\omega,\bar{Z})}\dfrac{1}{(1-\bar{U}\cos\theta)^2}\dfrac{D_j}{t_o}. & \text{2D} \end{array} \right. \tag{55}$$

Here $\bar{W}_o = D_j W_o$ is dimensionless, and derivatives present in the Wronskian are now evaluated with respect to the normalized distance $\eta$. Factor $(D_j / t_o)$ present in the 2D solution implies that the pressure field is evaluated per unit flow thickness $t_o$ in $x_2$ direction. Since the Wronskian in equation (23a) is independent of normal distance to the wall, computationally it is advantageous if it were evaluated at infinity where $V_2$ may be eliminated from the solution

$$\frac{b_2(\vec{k}_t^*,\omega)}{W_o(\vec{k}_t^*,\omega,\bar{Z})} = -\left[\frac{e^{iD_j\chi_\infty\eta}}{iD_j\chi_\infty V_1(\vec{k}_t^*,\eta,\omega)+V_1'(\vec{k}_t^*,\eta,\omega)}\right]_{\eta\to\infty} . \quad (56)$$

***Sample Computations***

We start with a rigid boundary condition on the wall ($\bar{Z}\to\infty$) and a set of values for the observer location and flow condition as ($\phi=\pi/2, \theta=\pi/4, St_o=0.30, U_j/c_\infty=0.90, T_R=3.0$). Two linearly independent solutions $V_1$ and $V_2$ to equation (23a) are shown in Figures 7 and 8. The first solution $V_1$ is real, and possesses a relatively larger amplitude. The second solution $V_2$ is complex, and is solved subject to specified boundary conditions at $\eta=0$ and $\infty$. The missing initial boundary condition is solved as $V_2'(0)=(7.15751, 0.06114\,i)$. At large distance $\eta$ from the boundary, both $V_1$ and $V_2$ exhibit an oscillatory behavior with a regular period equal to $2\pi/(-D_j\chi_\infty)$.

Constant $b_2$ is determined from Eq. (29) as $\eta\to\infty$. Figure 9 shows that $b_2=(-0.18368, -0.13127\,i)$. The real and imaginary components of $G_N(\eta,\omega)$ are presented in Fig. 10. Since the far-field pressure is evaluated according to equation (44) as the convolution of the source correlation function and the GF, the importance of the GF appears only where the source density is not insignificant. This, most likely, is limited to the initial several diameters normal to the wall where jet/wall turbulence and/or heat related sources are present. Figure 11 displays an expanded view of the GF within the first 2 diameters normal to the wall. The amplitude is relatively larger at $\eta=1$ compared to regions within the TBL, and the phase is constant at 0.623 *Rad*.

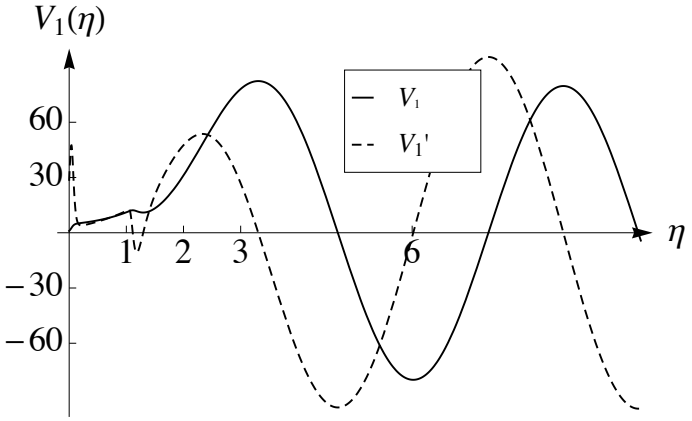


**Figure 7. Solution $V_1(\eta)$ (solid line) and its derivative (dashed line) subject to the mean velocity and temperature profiles of Figs 5 and 6 at $(\phi=\pi/2, \theta=\pi/4, St_o=0.30, U_j/c_\infty=0.90, T_R=3.0)$.**

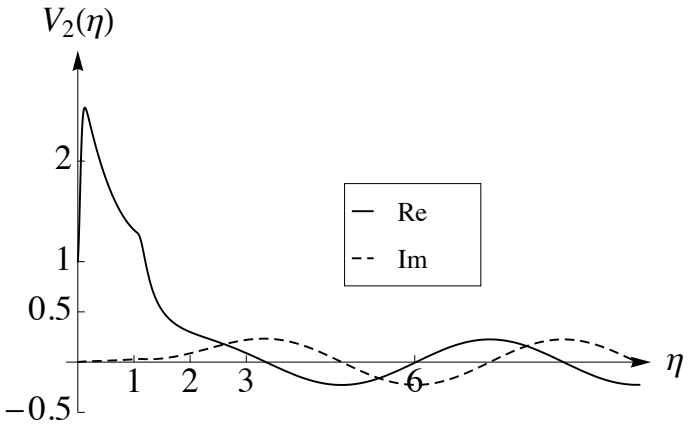


**Figure 8. Real (solid line) and imaginary (dashed line) components of solution $V_2(\eta)$ subject to the mean flow profiles of Figs 5 and 6 at $(\phi = \pi/2, \theta = \pi/4, St_o = 0.30, U_j/c_\infty = 0.90, T_R = 3.0)$.**

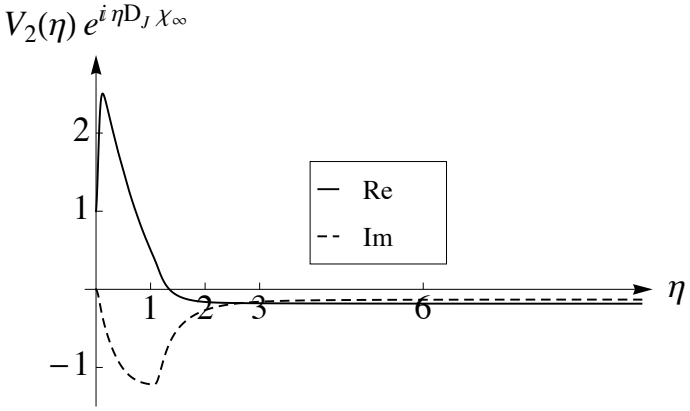


**Figure 9. Real (solid line) and imaginary (dashed line) components of constant parameter $b_2$ as $\eta \to \infty$.**

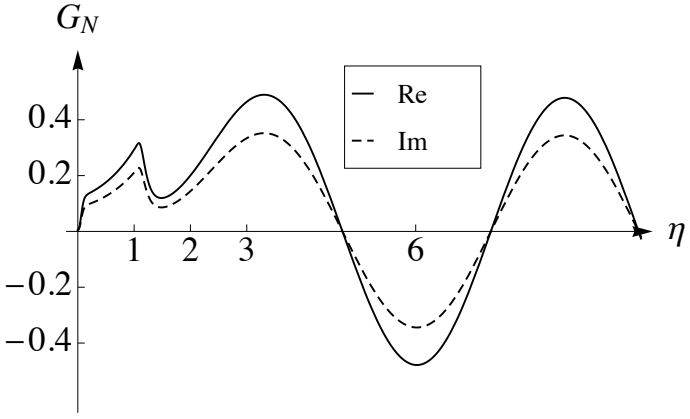


**Figure 10. Real (solid line) and imaginary (dashed line) components of the Green's function $G_N(\eta, \omega)$ at $(\phi = \pi/2, \theta = \pi/4, St_o = 0.30, U_j/c_\infty = 0.90, T_R = 3.0)$.**

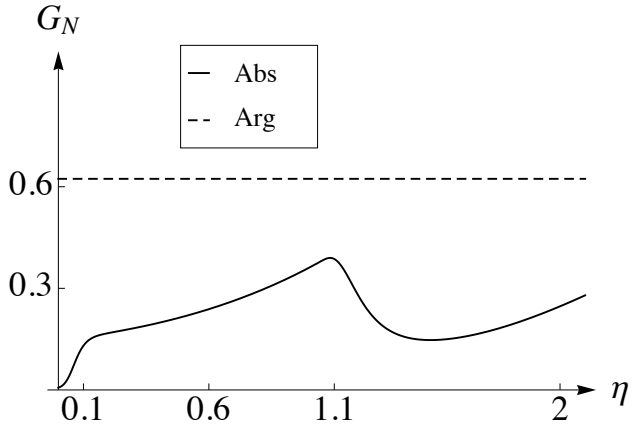


**Figure 11. Magnitude (solid line) and phase (dashed line) of the Green's function $G_N(\eta,\omega)$ at $(\phi=\pi/2, \theta=\pi/4, St_o=0.30, U_j/c_\infty=0.90, T_R=3.0)$.**

Next, we increase the frequency to $St_o=1.0$ while the remaining parameters are kept the same as before. Noticeable reduction in the magnitude of the GF (see Fig. 12) indicates that sound generation within the TBL should be minimal relative to the previous example at $St_o=0.30$ provided that the source densities remain comparable.

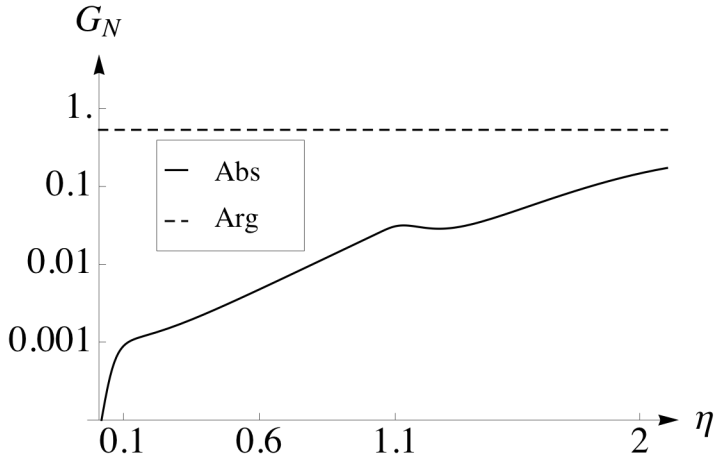


**Figure 12. Magnitude (solid line) and phase (dashed line) of the GF at $St_o=1.0$ – with the remaining parameters the same as in Fig. 11.**

In the third example, temperature effect is examined by considering an unheated jet at $T_R=1.0$, while the remaining parameters are kept the same as in Fig. 11. The temperature profile for this flow is seen in Fig. 13, and the corresponding GF solution is presented in Fig. 14. The magnitude of the GF at and near the wall ($\eta<1.1$) is increased considerably (nearly four times) relative to the heated jet shown in Fig. 11. It is noted that according to equation (55), that temperature effect enters the computations through factors $(c_\infty/c)$ as well as solution $V_1(\eta)$.

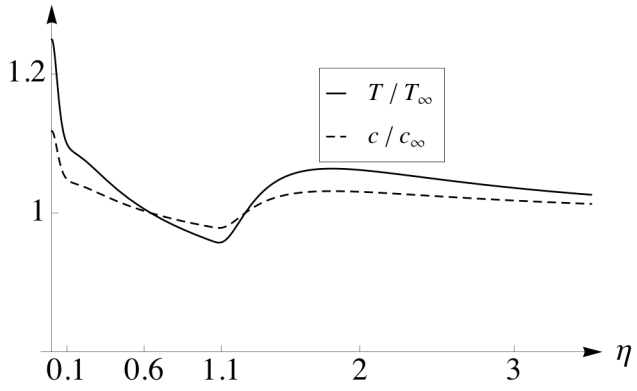


**Figure 13. Mean flow profiles for temperature (solid line) and sound speed (dashed line) in the unheated jet at $T_R$=1.0.**

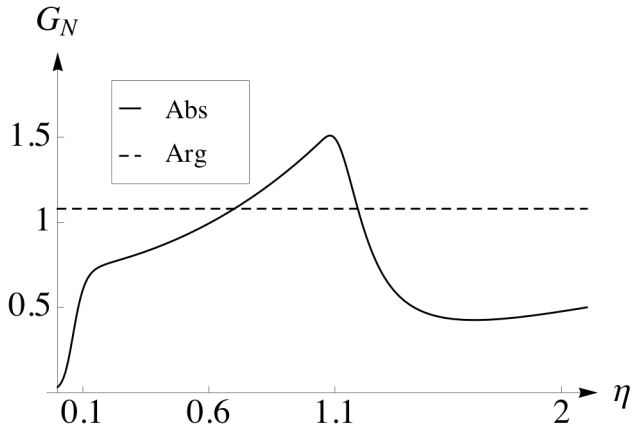


**Figure 14. Magnitude (solid line) and phase (dashed line) of the Green's function $G_N(\eta,\omega)$ at $(\phi=\pi/2, \theta=\pi/4, St_o$=0.30, $U_j/c_\infty$= 0.90, $T_R$ = 1.0).**

The effect of the observer location on the GF is examined by considering a polar angle of $\theta=\pi/2$ while the remaining parameters are kept the same as in example 1. Figure 15 shows an increase in the amplitude of the GF in a direction normal to the plate. In particular, there is substantial increase in the magnitude of the GF within the BL at $\eta<0.13$.

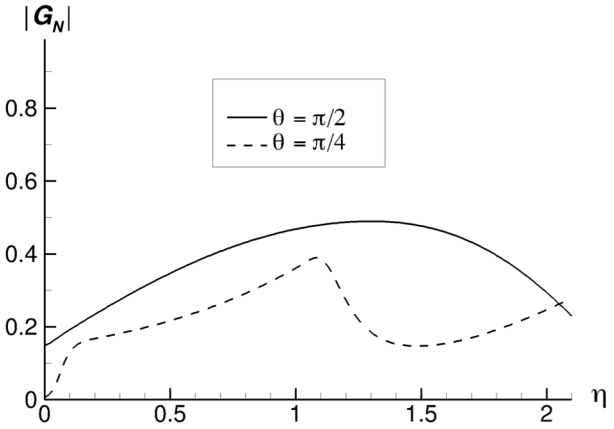


**Figure 15. Magnitude of the Green's function $G_N$ at $\theta=\pi/2$ (solid line), and $\theta=\pi/4$ (dashed line), at conditions of Fig. 11.**

The effect of wall conditions may be examined by selecting numerical values for the normalized impedance function $\bar{Z}$. The real and imaginary components of the surface impedance depend not only on the wall conditions, but also on the external flow characteristics such as Mach number and sound frequency and amplitude [Refs. 24, 25]. Aside from the solid boundary conditions ($\bar{Z} \to \infty$) examined earlier, here we choose a pair of values for the specific resistance and reactance as $\bar{Z} = (1 \pm 0.50i)$. Computational results are shown in figure 16 at unheated conditions $T_R = 1.0$, and at a polar angle of $\theta = \pi/4$. The amplitude of the GF is affected slightly, and only within the first diameter normal to the wall. The phase (shown in radians) remains constant for the rigid wall, but becomes a function of the source location when the impedance function consists of a reactive component.

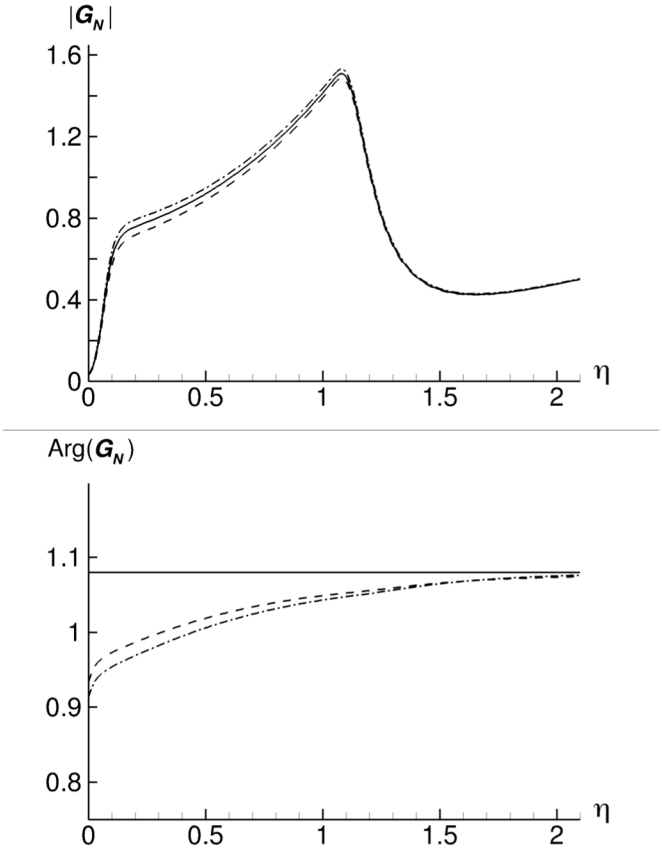


**Figure 16. The effect of wall impedance on the magnitude (top) and phase (bottom) of the GF – (rigid: solid line); (1 +0.50 i : dashed line); and (1 – 0.50 i : dash-dot) at** $(\phi = \pi/2, \theta = \pi/4, St_o = 0.30, U_j/c_\infty = 0.90, T_R = 1.0)$.

## 7.0 Summary

Prediction of the aircraft noise due to the interaction of the jet exhaust with a nearby solid surface is of increasing interest in the design of future civil transport. Concepts such as hybrid wing body aircraft, over the wing engine mount, or distributed propulsion are likely to contribute to jet surface interaction noise. While nearby surfaces could provide significant noise shielding

in certain directions, they also increase noise in other directions. In this study, we presented a formal solution to the propagation Green's function applicable to a rectangular jet exhaust in the proximity of a flat surface. The governing equation is the compressible Pridmore-Brown equation. Both frictional heat generation and thermal gradients in the boundary layer are potential contributors to noise generation and propagation. The general expression for the far-field noise (eq. 42) resembles that in the absence of a nearby surface – the major difference is concealed in the propagator, which should now be evaluated subject to prescribed boundary conditions on the surface. It was pointed out that aside from the scrubbing noise, scattered noise (or trailing edge noise) is also present on both side of the surface. A comprehensive prediction model needs to account for both noise components.

Numerical results were presented that show a parametric study of the propagation Green's function at selective values of the source frequency, jet temperature, observer angle, and wall impedance function using analytical representations of the mean flow profiles. For round jets, a conformal mapping to a rectangular strip needs to be carried out. In practice, a Reynolds-Averaged Navier-Stokes solution to the nozzle flow in the proximity of the surface (with an appropriate turbulence model) provides the mean flow and turbulence information required for modeling both momentum-flux and enthalpy-flux source components. The propagation equation should be solved numerically at each pair of observer angles $(\theta, \phi)$, and at each frequency $\omega$ subject to the *local* mean velocity and density profiles. In a 2D formulation, the GF is evaluated according to equation (51) while the mean flow is considered as a superposition of parallel slices in $x_1$ direction and infinitely long in $x_2$ direction. When the locally parallel flow approximation is extended to $x_2$ direction the GF is evaluated according to equation (39). Here, the jet may be sub-divided into elements in the span-wise $x_2$ direction in order to account for a finite wetted domain with an eventual decay of the source density in this direction.

**Nomenclature**

| | |
|---|---|
| $b_2$ | Far field amplitude (eq. 29) |
| $c$ | Sound speed |
| $D_j$ | Jet Diameter |
| $\delta_o$ | Boundary layer thickness |
| $\eta$ | Normalized distance $y_3 / D_j$ |
| $G$ | Green's function |
| $\hat{G}, \breve{G}$ | Transformed Green's function |
| $G_N$ | Normalized Green's function |
| $h'$ | Enthalpy fluctuations |
| $h$ | Enthalpy |
| $h'_o$ | moving frame stagnation enthalpy ( $h' + v'_j v'_j / 2$ ) |

| | |
|---|---|
| $\eta$ | Normalized distance from the wall |
| $\gamma$ | Specific heats ratio |
| $\Gamma$ | Source |
| $\vec{k}$ | Wave number |
| $k_t$ | Wave number vector $(k_1, k_2)$ |
| $\kappa_o$ | Wave number magnitude $(\omega / c_\infty)$ |
| $M$ | Mach number $(U / c)$ |
| $\omega$ | Radian frequency $(2\pi f)$ |
| $\pi'$ | Normalized pressure fluctuation |
| $p'$ | Acoustic pressure |
| $P(k_t, \omega)$ | Wall-pressure wave number-frequency spectrum |
| $q(\vec{y}, \vec{\xi}, \tau)$ | Source correlation function |
| $\rho$ | Density |
| $R$ | Distance $\lvert\vec{x} - \vec{y}\rvert$ |
| $\vec{\xi}$ | Spatial separation vector |
| $\psi$ | Wall function (eq. 21b) |
| $t$ | Time |
| $T_R$ | Stagnation temperature ratio |
| $\tau$ | Time delay |
| $U$ | Mean axial velocity |
| $U_e$ | Peak velocity in the boundary layer |
| $v_i'$ | Turbulent velocity component |
| $\tilde{v}_i$ | Mass-averaged velocity component |
| $\theta$ | Polar angle |
| $\phi$ | Azimuthal angle |
| $W_o$ | Wronskian |
| $\vec{x}$ | Rectangular coordinates |
| $\vec{y}$ | Source location |
| $\overline{Z}$ | Surface impedance |

Subscripts

| | |
|---|---|
| $o$ | At the surface variable |
| $\infty$ | Ambient condition |

Superscripts

| | |
|---|---|
| – | Time average |
| ^ | Fourier transformed variable |
| ~ | Favre average $(\tilde{q} = \overline{\rho q} / \overline{\rho})$ |

**Appendix-A Influence of the Solid Surfaces**

The Navier-Stokes equations when linearized about a non-radiating base flow may be written as a set of five linear equations [Ref. 15]

$$L_{\nu\mu}u_{\mu} = f_{\nu}(\vec{x},t)\,, \qquad (\mu,\nu = 1,2,...,5) \tag{A1}$$

where $u_{\mu}$ denotes the five dependent variables

$$\begin{aligned} &u_{\mu} = (m_i, p'_e, \rho') \\ &m_i = \rho v'_i, \quad i = 1,2,3 \end{aligned} \tag{A2}$$

(Latin indices repeat from 1 to 3, and Greek indices repeat from 1 to 5). The first three equations in (A1) correspond to the linearized momentum equation, followed by the energy and mass equations in the fourth and fifth place. The Green's Function (GF) to set of equations (A1) with a non-zero delta function source placed in the $\sigma th$ equation is denoted as $g_{\mu\sigma}$

$$L_{\nu\mu}g_{\mu\sigma}(\vec{x},t\,|\,\vec{y},\tau) = \delta_{\nu\sigma}\delta(\vec{x}-\vec{y})\delta(t-\tau). \tag{A3}$$

The source term appearing on the right hand side of (A1) is

$$f_{\nu}(\vec{x},t) = \frac{\partial}{\partial x_j}e''_{\nu j} + \delta_{\nu 4}(\gamma-1)e''_{ij}\frac{\partial \tilde{v}_i}{\partial x_j}, \quad (i,j = 1,2,3), \quad \nu = 1,\ldots,5 \tag{A4}$$

$$\begin{aligned} &e''_{\nu j} = -(\rho v'_{\nu}v'_j - \overline{\rho v'_{\nu}v'_j}), \\ &v'_4 = (\gamma-1)(h' + \frac{1}{2}v'^2), \quad v'_5 = 0. \end{aligned} \tag{A5}$$

The first three source components relate to difference between momentum flux terms and their Favre-averaged values, while the fourth term is related to the enthalpy flux and its Favre-averaged value, and the fifth source term (mass equation) is obviously zero.

Note that both momentum variable $m_i$ and pressure variable $p'_e$ are non-linear, however, in practice we set $m_i \simeq \bar{\rho}v'_i$, and

$$p'_e = p' - \frac{(\gamma-1)}{2}e''_{kk}\,, \tag{A6}$$

implies that $p'_e \simeq p'$ in the acoustic domain where turbulence is zero.

The field variables of interest are obtained from equations (A1) and (A3) using the source/GF convolution integral

$$u_\mu(\vec{x},t) = \int_\tau \int_{\vec{y}} g_{\mu\nu}(\vec{x},t \mid \vec{y},\tau) f_\nu(\vec{y},\tau) d\vec{y} d\tau, \tag{A7}$$

For example, when $\mu = 4$ the far-field acoustic pressure is evaluated as

$$p'(\vec{x},t) \approx p'_e(\vec{x},t) = \int_\tau \int_{\vec{y}} g_{4\nu}(\vec{x},t \mid \vec{y},\tau) f_\nu(\vec{y},\tau) d\vec{y} d\tau \ . \tag{A8}$$

Considering that $f_5 = 0$, the latter operation requires solving (A3) four times, each time by placing a delta function in the one of the first four equations. This process would also solve for other GF components that are not necessary for the purpose of evaluating $p'$. It is computationally advantageous if the field variables were evaluated from the set of the adjoint equations that are governed by

$$L^{(a)}_{\nu\mu}\ g^{(a)}_{\mu\sigma}(\vec{x},t \mid \vec{y},\tau) = \delta_{\nu\sigma}\delta(\vec{x}-\vec{y})\delta(t-\tau). \tag{A9}$$

The adjoint operator (denoted by superscript *a*) is readily evaluated once we multiply equation (A1) by $g^{(a)}_{\nu\sigma}(\vec{x},t \mid \vec{y},\tau)$, and rearrange its left hand side to appear as

$$g^{(a)}_{\nu\sigma}(\vec{x},t \mid \vec{y},\tau) L_{\nu\mu} u_\mu(\vec{x},t) = u_\mu(\vec{x},t) L^{(a)}_{\mu\nu}\, g^{(a)}_{\nu\sigma}(\vec{x},t \mid \vec{y},\tau) + \frac{\partial}{\partial t}\left(u_\mu g^{(a)}_{\mu\sigma}\right) + \frac{\partial}{\partial x_j} F_{j\sigma}. \tag{A10}$$

The last two terms on the RHS of (A10) represent the bi-linear form of $u_\mu$ and $g^{(a)}_{\mu\sigma}$, and

$$F_{j\sigma}(\vec{x},t \mid \vec{y},\tau) = \tilde{v}_j(\vec{x},t) u_\mu(\vec{x},t) g^{(a)}_{\mu\sigma}(\vec{x},t \mid \vec{y},\tau) + u_4 g^{(a)}_{j\sigma} + u_j\left(g^{(a)}_{5\sigma} + c^2 g^{(a)}_{4\sigma}\right). \tag{A11}$$

We solve for $u_\sigma(\vec{y},\tau)$ by placing (A9) into (A10), and integrating this equation within a large four-dimensional space-time volume $(\vec{x},t)$ surrounding the source

$$\int_t \int_{\vec{x}} g^{(a)}_{\nu\sigma}(\vec{x},t \mid \vec{y},\tau) f_\nu(\vec{x},t)\, d\vec{x}\, dt = u_\sigma(\vec{y},\tau) + \int_t \int_{\vec{x}} \left( \frac{\partial}{\partial t}\left(u_\mu g^{(a)}_{\mu\sigma}\right) + \frac{\partial}{\partial x_j} F_{j\sigma} \right) d\vec{x} dt. \tag{A12}$$

Following the divergence theorem, the volume integral on the RHS of (A12) may be converted into a surface integral. When there are no solid surfaces to interfere with the sound, this integral is evaluated on the surface of a large 4D sphere in $(\vec{x},t)$ domain – resulting in a null contribution due to the vanishing of the field variables $u_\mu$ on such a surface. Consequently (A12) becomes

$$u_\mu(\vec{x},t) = \int_\tau \int_{\vec{y}} g^{(a)}_{\nu\mu}(\vec{y},\tau \mid \vec{x},t) f_\nu(\vec{y},\tau) d\vec{y} d\tau. \qquad \text{(No solid surfaces)} \tag{A13}$$

Equations (A7) and (A13) point to the reciprocity of the GF in the absence of solid surfaces, i.e.,

$$g^{(a)}_{\nu\mu}(\vec{y},\tau \mid \vec{x},t) = g_{\mu\nu}(\vec{x},t \mid \vec{y},\tau)\,. \tag{A14}$$

By setting $\mu = 4$ we evaluate the far-field pressure. It is seen that the advantage of (A13) over (A7) is that we now place a source only in the fourth equation within set (A9) to compute the required GF components for pressure. Equation (A13) represents the fundamental solution to the governing equations. In the presence of solid boundaries in a finite domain, the general solution, when formulated in terms of the adjoint GF, is complemented with surface integrals as shown in (A12). The reciprocity condition (A14) would not necessarily be satisfied when reflecting boundaries are present in the acoustic medium unless surface integrals are forced to disappear by imposing conditions on the adjoint GF.

To investigate the surface integrals further, we allow volume $\vec{x}(t)$, externally and/or internally, be bounded by surface $s(t)$ with a unit outward normal $\vec{n}$ (Fig. A1). The first term within the bracket on the RHS of (A12) is expressed as the sum of two terms following the Leibniz's rule

$$\int_{\vec{x}(t)} \frac{\partial}{\partial t}\left(u_\mu g^{(a)}_{\mu\sigma}(\vec{x},t \mid \vec{y},\tau)\right) d\vec{x} = \frac{d}{dt}\int_{\vec{x}(t)} u_\mu g^{(a)}_{\mu\sigma}(\vec{x},t \mid \vec{y},\tau) d\vec{x} - \int_{s(t)} \vec{n}\cdot\vec{V}^s u_\mu g^{(a)}_{\mu\sigma}(\vec{x},t \mid \vec{y},\tau) ds \ . \tag{A15}$$

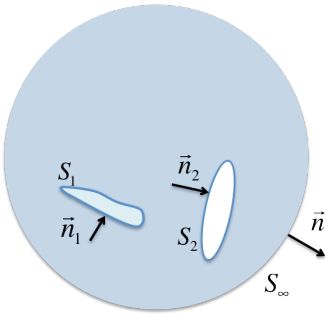


**Figure A1. Solid surfaces within the acoustic medium**

where $\vec{V}^s(\vec{x},t)$ is the velocity at an arbitrary point on the surface $s(t)$. We now integrate both sides of (A15) within the time interval [-T, T] for some large time T. The first terms on the RHS of (A15) vanishes due to the initial condition (in a remote past time), and the causality condition. Inserting (A15) into (A12) and applying the divergence theorem to the last term in (A12), we find (upon interchanging dummy variables)

$$u_\mu(\vec{x},t) = \int_\tau \int_{\vec{y}} g^{(a)}_{\nu\mu}(\vec{y},\tau \mid \vec{x},t) f_\nu(\vec{y},\tau) d\vec{y} d\tau + \int_{-T}^{T} d\tau \int_{s(\tau)} n_j \left[V^s_j u_\nu g^{(a)}_{\nu\mu}(s,\tau \mid \vec{x},t) - F_{j\mu}(s,\tau \mid \vec{x},t)\right] ds \tag{A16}$$

Integral equation (A16) represents a formal solution to the problem. The two integrals represent contributions to the acoustic field due to the volume and surface sources, respectively. In particular, the acoustic pressure is solved when $\mu = 4$. Moving the partial derivatives from

source to the GF and/or imposing boundary conditions on the surface integrals may achieve further simplifications. For example, placing $f_v$ from (A4) into (A16), and using the identity

$$g_{v\mu}^{(a)}(\vec{y},\tau\,|\,\vec{x},t)\frac{\partial}{\partial y_j}e_{vj}'' = \frac{\partial}{\partial y_j}\left(g_{v\mu}^{(a)}(\vec{y},\tau\,|\,\vec{x},t)e_{vj}''\right) - e_{vj}''\frac{\partial}{\partial y_j}g_{v\mu}^{(a)}(\vec{y},\tau\,|\,\vec{x},t)$$

followed by application of the divergence theorem on the first term on the right shows that

$$\begin{aligned} u_\mu(\vec{x},t) = &-\int_\tau\int_{\vec{y}}\left(\frac{\partial g_{v\mu}^{(a)}}{\partial y_j} - (\gamma-1)\frac{\partial \tilde{v}_v}{\partial y_j}g_{4\mu}^{(a)}\right)e_{vj}''(\vec{y},\tau)d\vec{y}d\tau + \int_{-T}^{T}d\tau\int_s n_j g_{v\mu}^{(a)}(s,\tau\,|\,\vec{x},t)e_{vj}''dsd\tau \\ &+\int_{-T}^{T}d\tau\int_s n_j\left[V_j^s u_v g_{v\mu}^{(a)}(s,\tau\,|\,\vec{x},t) - F_{j\mu}(s,\tau\,|\,\vec{x},t)\right]ds. \end{aligned} \tag{A17}$$

Further, substituting for $F_{j\mu}$ from (A11) into this last expression and imposing the no-slip boundary condition on a hard surface

$$(V_j^s - \tilde{v}_j).n_j = 0\ , \tag{A18}$$

results in the following integral equation for pressure

$$\begin{aligned} p_e'(\vec{x},t) = &-\int_\tau\int_{\vec{y}}\Gamma_{vj}^{(a)}(\vec{y},\tau\,|\,\vec{x},t)e_{vj}''(\vec{y},t)d\vec{y}d\tau + \int_{-T}^{T}d\tau\int_s n_j g_{v4}^{(a)}(s,\tau\,|\,\vec{x},t)e_{vj}''ds \\ &-\int_{-T}^{T}d\tau\int_s n_j\left[p_e'(s,\tau)g_{j4}^{(a)}(s,\tau\,|\,\vec{x},t) + m_j(s,\tau)(g_{54}^{(a)} + c^2 g_{44}^{(a)})\right]ds \end{aligned} \tag{A19}$$

where

$$\Gamma_{vj}^{(a)} \equiv \frac{\partial g_{v4}^{(a)}}{\partial y_j} - (\gamma-1)\frac{\partial \tilde{v}_v}{\partial y_j}g_{44}^{(a)}\ . \tag{A20}$$

**Appendix-B Vanishing of the Surface Integrals**

Here we show that the boundary condition (21) eliminates the surface integrals in the Green's function formulation of the acoustic field for bounded media. We start with equation (1), and apply Fourier transform with respect to variables $x_1$, $x_2$ and $t$ as defined in eq. (7) with the over hat carrot denoting a transformed variable

$$\frac{\partial^2 \hat{\vartheta}}{\partial x_3^2} + f(\vec{k}_t, x_3, \omega)\hat{\vartheta} = \hat{\Lambda}, \tag{B1}$$

where function $f$ was defined in eq. (11) and

$$\hat{\vartheta}(\vec{k}, x_3, \omega) \equiv \hat{\pi}'(\vec{k}_t, x_3, \omega)\frac{c(x_3)}{-\omega + k_1 U(x_3)}, \quad \hat{\Lambda}(\vec{k}, x_3, \omega) \equiv \frac{i\hat{\Gamma}}{c(x_3)\left(-\omega + k_1 U(x_3)\right)^2}. \tag{B2}$$

Multiply eq. (9) by $\hat{\vartheta}$, and equation (B1) by $\breve{G}$, subtract the two expressions, and integrate the result with respect to $x_3$

$$\int_0^\infty \left( \breve{G}\frac{\partial^2 \hat{\vartheta}}{\partial x_3^2} - \hat{\vartheta}\frac{\partial^2 \breve{G}}{\partial x_3^2} \right) dx_3 = \int_0^\infty \left( \breve{G}\hat{\Lambda} - \hat{\vartheta}\,\delta(x_3 - y_3) \right) dx_3, \tag{B3}$$

or

$$-\left( \breve{G}\frac{\partial \hat{\vartheta}}{\partial x_3} - \hat{\vartheta}\frac{\partial \breve{G}}{\partial x_3} \right)\Bigg|_0^\infty = \hat{\vartheta}(\vec{k}, y_3, \omega) - \int_0^\infty \breve{G}(\vec{k}_t, x_3, y_3, \omega)\hat{\Lambda}(\vec{k}, x_3, \omega) dx_3 \ . \tag{B4}$$

Upon recognizing that $\partial\hat{\vartheta}/\partial x_3 = -i\chi_\infty \hat{\vartheta}$, and $\partial\breve{G}/\partial x_3 = -i\chi_\infty \breve{G}$ at infinity, the upper limit of the expression on the left hand side of (B4) vanishes. On the right, since the GF is self-adjoint we switch $x_3$ and $y_3$ in the argument of $\breve{G}$, and subsequently we substitute expressions for $\hat{\Lambda}$ from (B2), and $\breve{G}$ from (10) into (B4) to show that in view of (19), the right hand side of this equation also vanishes.

Consequently we arrive at

$$\breve{G}\frac{\partial \hat{\vartheta}}{\partial x_3} - \hat{\vartheta}\frac{\partial \breve{G}}{\partial x_3} = 0, \quad x_3 = 0 \ . \tag{B5}$$

Using surface boundary condition (18) in (B5) shows that

$$\frac{\partial \breve{G}}{\partial x_3} - \psi\breve{G} = 0, \qquad x_3 = 0 \tag{B6}$$

where function $\psi(k_1, \omega, \bar{Z})$ is given in (21b).

## References


[1] Brown, C. A., "Jet-Surface interaction test: far-field noise results," ASME paper GT2012-69639, June 2012.

[2] Podboy, G. G., "Jet-Surface interaction test: phased array noise source localization results," ASME paper GT2012-69801, June 2012.

[3] FFowcs Williams, J. E., and Hall, L. H., "Aerodynamic sound generation by turbulent flow in the vicinity of a scattering half plane," J. Fluid Mechanics, **40(4)**, (1970), pp. 657–670.

[4] Powell, Alan, "On the aerodynamic noise of a rigid flat plate moving at zero incidence," J. Acoustical Soc. Am., 31(12), (1959), pp. 1649-1653.

[5] Lawrence, J. L. T., Azarpeyvand, M., and Self, R. H., "Interaction between a flat plate and a circular subsonic jet, " AIAA paper AIAA-2011-2745, June 2011.

[6] Bowman, J. J., Senior, T. B. A., and Uslenghi, P. L. E., *Electromagnetic and Acoustic Scattering by Simple Shapes* (1987), Hemisphere Publishing Corp., New York.

[7] Howe, M. S., "A review of the theory of trailing edge noise," J. Sound and Vib. **61(3)**, (1978), pp. 437-465.

[8] Goldstein, M. E., "Scattering and distortion of the unsteady motion on transversely sheared mean flows," J. Fluid Mechanics, **91(4)**, (1979), pp. 601-632.

[9] Howe, M. S., "Surface pressure and sound produced by turbulent flow over smooth and rough walls," J. Acoustical Soc. Am., 90(2), (1991), pp. 1041-1047.

[10] Sevik, M. M., "Topics in hydrodynamics," *Proceedings of IUTAM Symposium*, Aero- and Hydrodynamics, Lyon (1985), Berlin: Springer-Verlag.

[11] Pridmore-Brown, D. C., "Sound propagation in a fluid flowing through an attenuating duct," J. Fluid Mech. **4**, (1958), pp. 393–406.

[12] Goldstein, M. E., "Relation between the generalized acoustic analogy and Lilley's contribution to aeroacoustics," International J. Aeroacoustics, **9(4, 5)**, (2010), pp. 401-418.

[13] Chase, D. M., and Noiseux, C. F., "Turbulent wall pressure at low wavenumbers: Relation to nonlinear source in planar and cylindrical flow," J. Acoust. Soc. Am., **72(3)**, (1982), pp. 975–982.

[14] Bark, F. H., "On the wave structure of the wall region of a turbulent boundary layer," J. Fluid Mechanics, **70**, (1975), pp. 229–250.

[15] Goldstein, M. E., "A generalized acoustic analogy," J. Fluid Mechanics, **488**, (2003), pp. 313-333.

[16] Chandiramani, K. L. "Diffraction of evanescent waves, with application to aerodynamically scattered sound and radiation from unbaffled planes," J. Acoustical Soc. Am. **55(1)**, (1974), pp. 19-29.

[17] Howe, M. S., "The displacement-thickness theory of trailing edge noise," J. Sound and Vib. **75(2)**, (1981), pp. 239-250.

[18] Jones, D. S., "The scattering of sound by a simple shear layer," Proc. Roy Soc. A, 284, (1977), pp. 287–328.

[19] Erdelyi, A., *Asymptotic Expansions* (2010), Dover Publications, Inc.

[20] Khavaran, A., Bridges, J., and Georgiadis, N., "Prediction of turbulence-generated noise in unheated jets," NASA/TM–2005-213827, 2005.

[21] Howe, M. S., "On the generation of sound by turbulent boundary layer flow over a rough wall," Proc. R. Soc. London, **A 395**, (1984), pp. 247-163

[22] FFowcs Williams, J. E., "Boundary layer pressure and the Corcos model: A development to incorporate low wavenumber constraints," J. Fluid Mechanics, **125**, (1982), pp. 9-25.

[23] Chase, D. M., "The character of turbulent wall pressure spectrum at sub-convective wavenumbers and a suggested comprehensive model," J. Sound and Vib. **(112)**, (1987), pp.125-147.

[24] Watson, W. R., Tracy, M. B., Jones, M. G., and Parrott, T. L., "Impedance eduction in the presence of shear flow," AIAA paper AIAA-2001-2263, May 2001.

[25] Malmary, C., Carbonne, S., Auregan, Y., and Pagneux, V., "Acoustic impedance measurement with grazing flow," AIAA paper, AIAA-2001-2193, May 2001.

| REPORT DOCUMENTATION PAGE | | | Form Approved OMB No. 0704-0188 |
|---|---|---|---|



| 1. REPORT DATE *(DD-MM-YYYY)* | 2. REPORT TYPE | 3. DATES COVERED *(From - To)* |
|---|---|---|
| 01-09-2013 | Final Contractor Report | |

| 4. TITLE AND SUBTITLE | 5a. CONTRACT NUMBER |
|---|---|
| Jet Surface Interaction--Scrubbing Noise | NNC12BA01B |
| | **5b. GRANT NUMBER** |
| | **5c. PROGRAM ELEMENT NUMBER** |
| **6. AUTHOR(S)** | **5d. PROJECT NUMBER** |
| Khavaran, Abbas | **5e. TASK NUMBER** |
| | **5f. WORK UNIT NUMBER** WBS 473452.02.03.07.06.01.02 |
| **7. PERFORMING ORGANIZATION NAME(S) AND ADDRESS(ES)** | **8. PERFORMING ORGANIZATION REPORT NUMBER** |
| Vantage Partners, LLC | E-18785 |
| **9. SPONSORING/MONITORING AGENCY NAME(S) AND ADDRESS(ES)** | **10. SPONSORING/MONITOR'S ACRONYM(S)** |
| National Aeronautics and Space Administration<br>Washington, DC 20546-0001 | NASA |
| | **11. SPONSORING/MONITORING REPORT NUMBER** NASA/CR-2013-218090 |

**12. DISTRIBUTION/AVAILABILITY STATEMENT**
Unclassified-Unlimited
Subject Category: 71
Available electronically at http://www.sti.nasa.gov
This publication is available from the NASA Center for AeroSpace Information, 443-757-5802

**13. SUPPLEMENTARY NOTES**

**14. ABSTRACT**
Generation of sound due to scrubbing of a jet flow past a nearby solid surface is investigated within the framework of the generalized acoustic analogy theory. The analysis applies to the boundary layer noise generated at and near a wall, and excludes the scattered noise component that is produced at the leading or the trailing edge. While compressibility effects are relatively unimportant at very low Mach numbers, frictional heat generation and thermal gradient normal to the surface could play important roles in generation and propagation of sound in high speed jets of practical interest. A general expression is given for the spectral density of the far-field sound as governed by the variable density Pridmore- Brown equation. The propagation Green's function should be solved numerically starting with the boundary conditions on the surface and subject to specified mean velocity and temperature profiles between the surface and the observer. The equivalent sources of aerodynamic sound are associated with non-linear momentum flux and enthalpy flux terms that appear in the linearized Navier-Stokes equations. These multi-pole sources should be modeled and evaluated with input from a Reynolds-Averaged Navier-Stokes (RANS) solver with an appropriate turbulence model.

**15. SUBJECT TERMS**
Acoustics; Noise; Jet noise; Propulsion noise

| 16. SECURITY CLASSIFICATION OF: | | | 17. LIMITATION OF ABSTRACT | 18. NUMBER OF PAGES | 19a. NAME OF RESPONSIBLE PERSON |
|---|---|---|---|---|---|
| a. REPORT | b. ABSTRACT | c. THIS PAGE | | | STI Help Desk (email:help@sti.nasa.gov) |
| U | U | U | UU | 38 | 19b. TELEPHONE NUMBER *(include area code)* 443-757-5802 |